Event-Driven Applications for Hard-Field Tomography Software Modelling of Forward and Inverse Solutions

Goh, C.L. [1], Ruzairi, A. R.[1,2,*], Abdullah, M. N[3], Hafiz, F. R. [4], Tee, Z.C.[5]

[1]Faculty of Electrical Engineering
  Universiti Teknologi Malaysia, Skudai, Johor, 81310, MALAYSIA.
[2]Faculty of Electrical and Electronic Engineering
  Universiti Tun Hussein Onn, Batu Pahat, Johor, 86400, MALAYSIA.
[3]Language Academy
  Universiti Teknologi Malaysia, Skudai, Johor, 81310, MALAYSIA.
[4]School of Mechatronic Engineering
  Universiti Malaysia Perlis, Arau, Perlis, 02600, MALAYSIA.
[5]LOGO Solution, Sdn. Bhd
  Masai, Johor, 81750, MALAYSIA.

Abstract: This paper addresses mathematical modelling for a tomography application, in which forward and inverse problems are discussed in detail in terms of the projection modelling and image reconstruction algorithm. The forward modelling of the ultrasonic prototype system is discussed to predict the sensor output for constructing cross-sectional images. Besides that, this paper also discusses the optimum image algorithm to solve the inverse problem for tomogram reconstruction. Event-driven software applications were designed as the solutions to both forward and inverse problems. The applications are discussed with the supporting programming flow charts. Simulations were performed in forward and inverse applications respectively, and results were analysed using an image quality assessment technique called the Mean Structural Similarity Index, MSSIM. The results which indicated high MSSIM (>90%) in image analysis concluded that the designed forward and inverse modelling applications can be deployed in real-time systems.

Keywords: Tomography; Modelling; Image Reconstruction; Mean Structural Similarity Index

1. Introduction

In industrial pipeline, tomography is a measurement technology for internal flow imaging. The use of sensors of any kind of penetrating wave in an industrial pipeline is termed as a tomograph, while the image produced based on the mathematical procedure called computed tomography (CT) reconstruction is a tomogram [1]. Fundamentally, a tomographic system deals with forward problems to model and estimate the theoretical sensor data readings of a tomograph, then the inverse problem is used to reconstruct a tomogram from its projections' sensor readings.

Generally, static sensitivity maps were plotted in previous tomography researches [2-6] as a working procedure of solving forward problems. Static sensitivity maps request the

pre-load of sensitivity values before running the tomogram application. Static sensitivity maps for all the projection paths are computationally very expensive since they require the inversion of a large array, and normally the sensitivity maps are drawn and pre-calculated in a separate software. The major disadvantage of static sensitivity maps is less flexibility in software application, where changing the image resolution will request a new generated map to be installed in the software. If there are any changes in sensor quantity or sensor projection angle, a new sensitivity map software or program need be regenerated. In this paper, the forward problem is structured based on the fan-beam ultrasonic tomography (UT) system, and inverse problem is discussed based on back projection image algorithms. We introduce and discuss the dynamic sensitivity check procedure and then provide the event-driven software

Corresponding author:ruzairi@uthm.edu.my
2011 UTHM Publisher. All right reserved.
penerbit.uthm.edu.my/ojs/index.php/ijie

16

application based on modelling principles. Finally, we present the analysis of the computed images.

2. Modelling Principles

In a transmission mode UT system, as of any other hard-field sensor concepts, it can be assumed that the wave propagation is in a straight-line form [7]. Fan beam projection geometry in the UT is the typical setup for bubble columns because of the sensor behavior [8]. In this study, the arrangement of sensor projection geometry consists of 16 sensors, equally arranged at the circumference around the bubble column. The sensor type chosen was the transceiver in which each sensor could be operated either as transmitter or receiver. The receivers were modelled as a circular arc, which receive a uniform ultrasonic energy in the liquid-gas flow column. In a 16 transceiver UT system, a complete scanning of the UT system takes a total of 16 projection cycles. In each scan, sensor S1 started the first cycle (S1 as transmitter, S2 to S16 as receivers), followed by sensor S2 (S2 as transmitter, S1, S3 to S16 as receivers), and until all sensors completed the projections before the next ultrasonic scan. Figure 1 shows a single projection of a fan-beam system while Figure 2 shows a complete scan in the fan-beam transmission mode UT system. This sensor geometry built the fundamentals of forward and inverse problem solvers for the image reconstruction algorithm of the developed UT system that will be explained in following section.
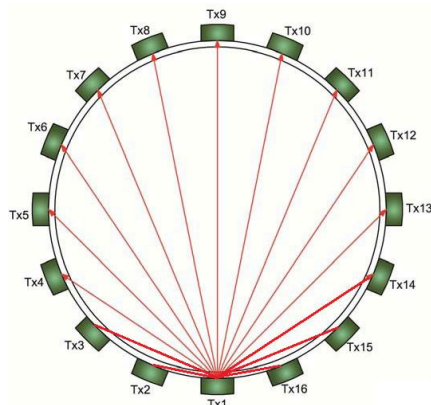

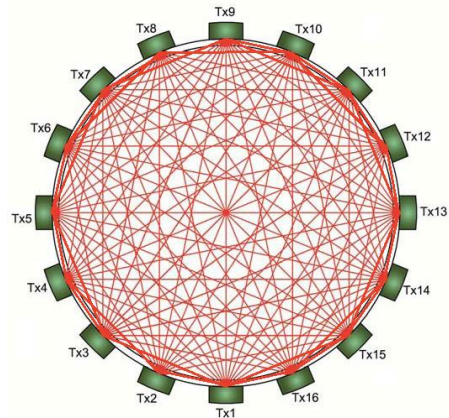Fig. 1 A Single Projection of a Fan-Beam System.

Fig. 2 A Complete Scan in a Fan-Beam System.

2.1 Forward Modelling

Forward problem was begun by modelling the deterministic aspects of the imaging system, the investigated cross-sectional area was superimposed as a square grid image plane and this discretization grid of image plane was set up by the ultrasonic transmission paths. The image plane was divided into small rectangles, which pixel was the smallest element in rectangle. The gridline mapping resolution was the software image resolution, (r x r pixels), as defined in the software drawing map as shown in Figure 3.
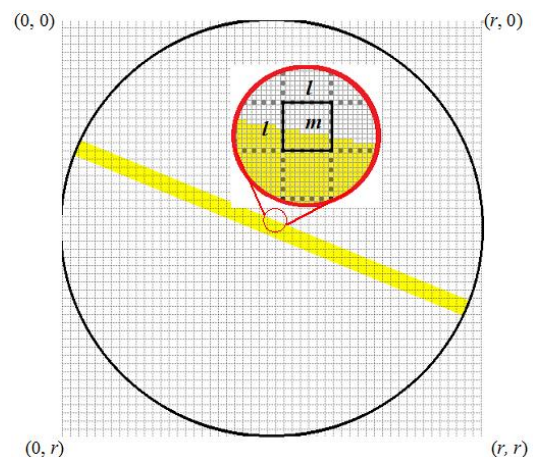

Fig. 3 Examples of Sensitivity Pixels on a Transmission Path.

Every transmission path had different sensitivity based on the gridline's mapping resolution. There was a number of pixels occupied in a transmission path, and each projection cycle consisted of a total of fifteen transmission paths based on the investigated fan-beam projection geometry. This resulted in

a series of sensitivity matrices depending on the image plane mathematical modelling in which sensitivity elements' value represents the number of pixels laid on the transmission path for corresponding elements. A higher the resolution (r) value formed a finer sensitivity matrices, and thus a better quality an image can be reconstructed [9]. An analytical solution using graphical programming technique was created for calculating the sensitivity matrices. The sensitivity matrices were generated to be a sensitivity map. The sensitivity map was formed by rectangular arrays, l x l pixels, in the mapping gridline. Value (l) represents the width of the transmission path in pixels count which can be defined using Equation 1.

Figure 3 shows a sample of a transmission path, from a specified transmitter, Si, to a specified receiver, Ri, was penciled in yellow (m pixels in the l x l rectangular array). The sensitivity value, S, for each the rectangular array (x, y) was obtained using Equation 2.

$$l = \frac{r}{16} \qquad (1)$$

$$S_{(Si,Ri)}(x, y) = \frac{m}{l^2} \qquad (2)$$

Equations 3 to 8 show the mathematical modelling procedures to generate the sensitivity lines of the dynamic sensitivity check; where d_j is the degree of the sensitivity line, SensorCnt is the number of sensor for the location (x_j, y_j), and i is the total number of sensors in the system. The value in degree was converted to radian, rad_j. Figure 4 shows the examples of constructed sensitivity linear lines during first projection cycle of sensor S_1. Linear line equations which were formed from Equations 3 to 8 were then structured in inverse modelling application to perform sensitivity checks. In the sensitivity checking procedure, every pixel in the image plane is coordinated by its own x and y value, and the 'view' intercepting the pixel each the projection was determined. A masking matrix, was defined in the dynamic software array to store the "view" results of each of the sensitivity checks.

$$d_j = SensorCnt \times \frac{360}{i} \qquad (3)$$

$$rad_j = \frac{d_j \times \Pi}{180} \qquad (4)$$

$$x_j = \frac{r}{2} \times \cos(rad_j) \qquad (5)$$

$$y_j = \frac{r}{2} \times \sin(rad_j) \qquad (6)$$

$$slope, M_j = \frac{Y_{j+1} - Y_j}{X_{j+1} - X_j} \qquad (7)$$

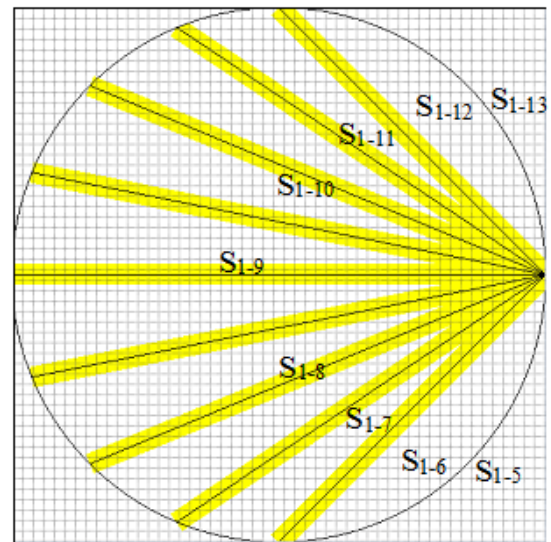$$Intercept, c_j = Y_j - M_j X_j \qquad (8)$$

Fig. 4 Transmission Paths of First Circle from a Sensor.

With the sensitivity information, forward problems could then be solved to obtain the theoretical sensor outputs using Equation 9, where Vg is the theoretical sensor loss voltage value, S is the sensitivity vector relating to the distributed image in the gridline, and G is the obstacles' image distribution vector in pixel value [10]. The forward problem determines the

theoretical output of each of the sensors when the ultrasonic transmission energy is attenuated by the gas bubbles in the sensing area [11 -12].

$$V_g = S \times G \qquad (9)$$

2.1.1 Event-Driven Application

In programming structure, forward modelling application was designed as an event driven application, and the software responded dependent on the interfaces controlled by user. Referring to Figure 5, there were two types of controls: the clickable button and display control.
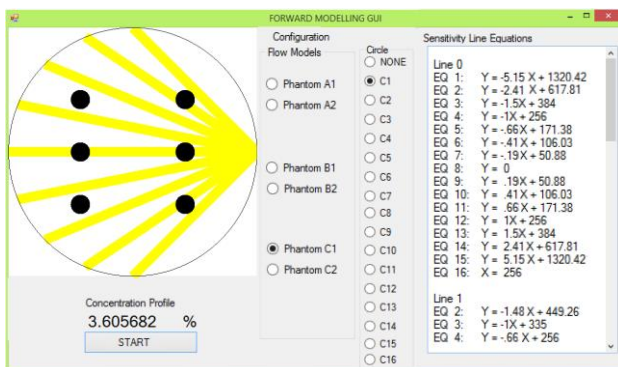

Fig. 5 Forward Modelling Application.

Through the radio buttons in the configuration box, the setting of the flow model and scanning circle could be selected by the user's preference. There was a total of nine predefined flow models (denoted as A1, A2, B1, B2, C1 and C2 phantoms). The flow models' radio buttons defined which of the phantoms were to be simulated into the tomogram. Meanwhile, the "Circle" radio buttons were used to define which projection scan was to be highlighted "yellow" on the simulated image. The forward modelling application operated after the user had clicked the "START" button. The forward modelling results were obtained in four ways: tomogram, numerical data, text file, and image file. The tomogram was displayed in the form of a two-dimensional plane on a running application. The concentration profile of the simulated phantom was displayed in the form of numerical data in

percentage value and sensitivity line equations for every transmission cycles were displayed in the form of numerical data in the "Sensitivity Line Equations" text box. After running the forward modelling software, the calculated sensitivity line equations were saved to a text file while the displayed image was saved as an image file. The image files were then processed to predict the theoretical sensor readings for each flow model. Figure 6 illustrates the overall flow chart for the software procedures in the forward modelling application.
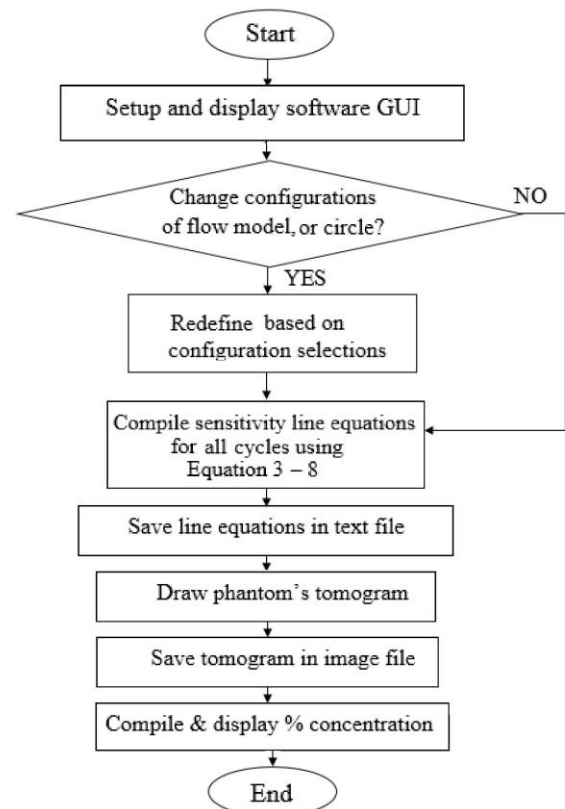

Fig. 6 Forward Modelling Flow Chart.

2.2 Inverse Modelling

There are numerous analytic solutions to solve the inverse problem to reconstruct an image from sensor readings. Back projection algorithm is popular among most of the researchers and thus it has many variations, basic practices are Linear Back Projection (LBP) and Filtered Back Projection (FBP). Ref. [13] and [14] discussed in detail the fundamental, mathematical modelling and procedures for back projection algorithms. LBP

algorithm has the advantage of low computation cost, and it does produce useful (albeit only 'qualitative') images [15]. The major limitation of the LBP algorithm is the blurry or ambiguous images due to the nonlinear sensing mechanism. In the LBP algorithm, the procedure is to multiply each sensor voltage reading, V_{Sn} by its sensitivity value, S_n, to produce the concentration profile in the matrices of m x [n x n], where m is the number of the obtained projection data while n is the reconstructed image resolution of the used sensitivity matrix [15]. A technique commonly used to improve LBP images is to use a filter, resulting in FBP. In FBP, a filter is introduced to overcome nonlinear or non-uniform sensor distribution. To offer a uniform concentration profile, this filter has the same dimensions as the sensitivity matrices to provide weighting to individual pixels. The filter is in the matrix format calculated by the ratio of maximum value measured in concentration sensitivity matrix, to each element in the overall full flow concentration sensitivity matrix. Hence, the computation of FBP concentration profile, V_{ij_FBP}, can be expressed mathematically as the filter matrix, multiplied by the LBP concentration detectable voltage, as shown in Equation 10 [4].

$$V_{ij\_FBP} = \sum_{n=1}^{n=16} \frac{V_{Sn}}{V_{\max_{Sn}}} \times V_{Sn} \times S_n \qquad (10)$$

As in forward modelling, dynamic sensitivity check through software programming was introduced in the inverse modelling. Approaching the standard FBP algorithm, Dynamic Filter Back Projection (D_FBP), Dynamic Hybrid Filter Back Projection (D_Hybrid_FBP) and Dynamic Hybrid Interpolation Filter Back Projection (D_Hybrid_IFBP) were derived based on the masking matrix, the programming array that stored the sensitivity value of each matric, M_{Sn}. Concentration profile of the D_FBP, $V_{ij\_D\_FBP}$, can be computed by multiplying the masking matrix with the corresponding filtered sensor reading as Equation 11.

$$V_{ij\_D\_FBP} = \sum_{n=1}^{n=16} M_{Sn} \times V_{ij\_FBP} \qquad (11)$$

Hybrid reconstruction technique enables a priori knowledge assuming binary value from the sensor, either zero for no material or one for the presence of material [15] to improve the accuracy of the image reconstruction by removing the noise pixels. Threshold ratio, η with respect to the maximum pixel value is used to define the presence of material as depicted in Equation 12.

$$V_{ij\_D\_Hybrid} = \left\{ \begin{array}{l} V_{ij\_D\_FBP} = 1; V_{ij\_D\_FBP} \geq \eta \\ V_{ij\_D\_FBP} = 0; V_{ij\_D\_FBP} < \eta \end{array} \right. \qquad (12)$$

Interpolation, also known as neighborhood averaging is a straightforward spatial-domain technique primarily for diminishing spurious effects in an image because of a poor transmission channel [16]. The integration technique to generate a smoothed image $G(x, y)$, where values at every point (x, y) are obtained by averaging the pixel values of a predefined neighborhood, $G'(x, y)$, of $V(x, y)$. Equation 13 and 14 shows the steps mathematically in the interpolation procedure. Both the Hybrid and interpolation techniques were integrated into the derived D_FBP image algorithm, resulting in D_Hybrid_FBP and D_Hybrid_IFBP.

$$G(x, y) = \left\{ \begin{array}{l} \frac{G'(x, y-1) + G'(x, y+1)}{2}; x = even, y = odd \\ \frac{G'(x-1, y) + G'(x+1, y)}{2}; x = odd \end{array} \right. \qquad (13)$$

$$G'(x, y) = V(\frac{x}{2}, \frac{y}{2}); x = even, y = even \qquad (14)$$

2.2.1   Event-Driven Application

In programming structure, Inverse modelling application was developed as event-driven application. In the inverse modelling application as shown in Figure 7, there were two data sources: online data (real-time sensor readings obtained from connected ultrasonic

hardware) and offline data (data that was saved from the real-time sensor system or forward modelling application). User could trigger the application software through user interfaces such as buttons, radio buttons and options in menu. The user interfaces were created for the purposes of starting the application, changing the programming running mode (offline or online), calibration configuration, tomogram algorithm, data loading, and data saving. After pressing the "START" button, the application software would be compiled according to the configurations. Any changes of the configurations (file menu, color bar menu, image resolution, image algorithm, programming mode, and calibration routine) would have to be interacted before pressing the "START" button. Once software in running mode, changes on configurations could only be made after a complete scanning compilation. Figure 8 illustrates the inverse modelling application with a complete data frame displayed as tomogram. Results of inverse modelling application were shown in numeric data and reconstructed image. The bubble concentration percentage and the system timing were both displayed in the numerical data form, text boxes of "Bubbly" and "Time" respectively. Figure 8 shows the overall programming flow chart for the inverse modelling application.
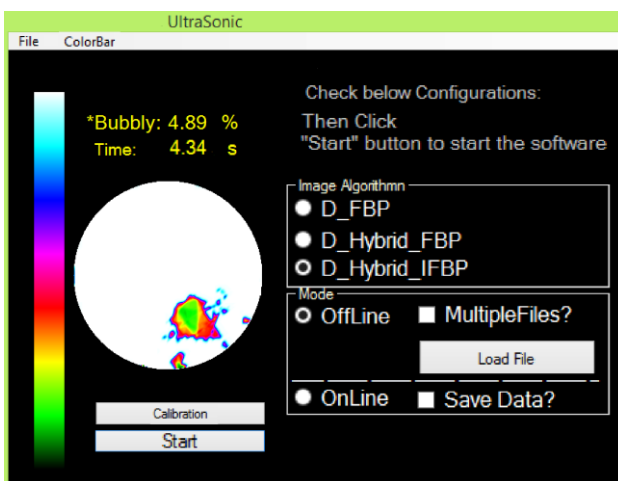
Fig. 7: Inverse Modelling Application.
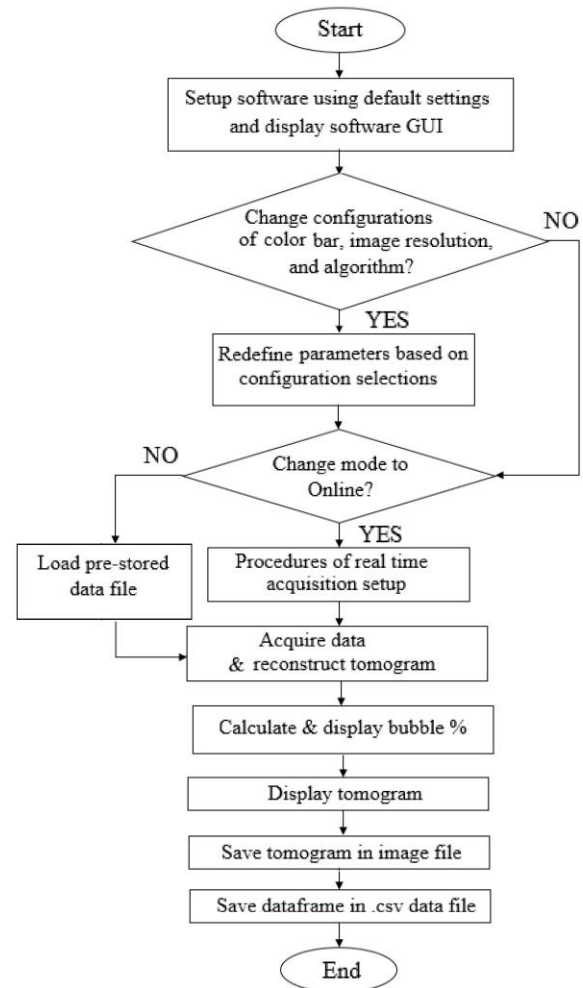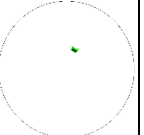

Fig. 8: Inverse Modelling Flow Chart.
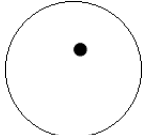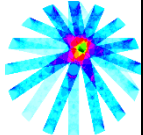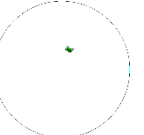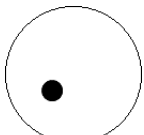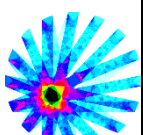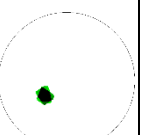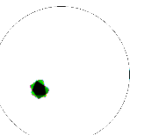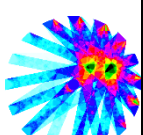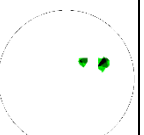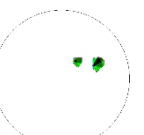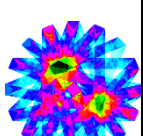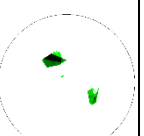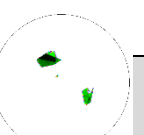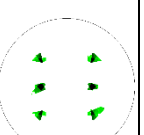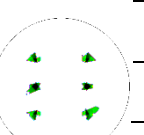
3. Results and Discussions

The forward modelling application is used to simulate objects based on different flow models and then predict the theoretical sensor readings. Then, the theoretical sensor readings can be fed to the inverse modelling software to reconstruct data into images through the coded image reconstruction algorithms. The purpose of doing so is to perform the image quality assessment between the simulated object and reconstructed object. From the results of image comparison, the ability and suitability of the event-driven programming application for 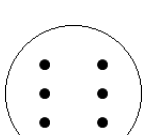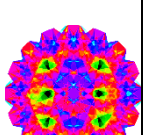the investigated tomography system can be verified. Table 1 tabulates the theoretical and reconstructed images from the forward and inverse modelling applications.

The reconstructed samples can be divided into three groups, namely single particle group A, double particle group B, and sparse particle

group C. From visual checking on the images reconstructed in Table 1, D_FBP resulted in smearing background noises, yet the locations of the particle/s could be identified. As shown in the results tabulated in Table 1, the Hybrid reconstruction technique was integrated into the back projection algorithm to improve the image accuracy by neglecting the blurry image, specifically the background noise, while the interpolation technique was integrated to acquire a neighborhood pixel smoothing effect with improved imaging spatial resolution.

Table 1 Tomograms with Various Image Algorithms.

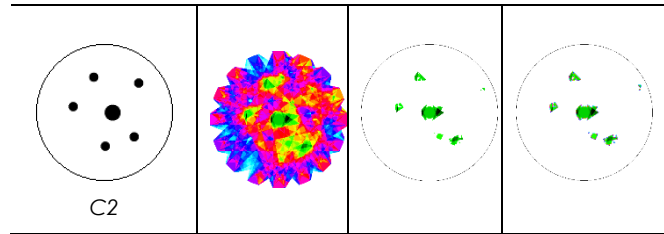| Forward Model (theoretical)	D_FBP Tomogram	D_Hybrid _FBP Tomogram	D_Hybrid _IFBP Tomogram
A1			
A2			
B1			
B2			
C1			

Image quality assessment provides quantitative measurements of an image; it is a method to compare the reconstructed (distorted) image to an original (distortion-free) image. Mean Structural Similarity Index, MSSIM, is a recent objective image quality assessment paradigm [17] to overcome the limitations of error sensitivity based image quality assessment techniques, which are Mean squared error, MSE, and peak signal-to-noise ratio, PSNR. Refer to numerous tests provided by previous researchers; MSSIM does a much better job at quantifying image quality than MSE or PSNR [18-20]. Higher MSSM index indicates better image quality. Governing equations of MSSIM can be found in [18]. Table 2 tabulated the MSSIM results for the reconstructed images. From the quantitative data, it was found that D_FBP resulted in poor MSSIM among the three image reconstruction techniques, with the worst images happening to group C, in which C1 and C2 scored only 43.18 % and 44.92% respectively. Quality of image improved significantly after implementing the Hybrid technique towards FBP algorithm, as the MSSIM for C1 and C2 increased to 95.26% and 94.73%, respectively. Tomograms reconstructed using Hybrid with or without interpolation techniques could meet the quality expectation as the MSSIM scored higher than 94% overall.

Table 2 MSSIM Results.

MSSIM	Flow Model					
	A1	A2	B1	B2	C1	C2
D_FBP, %	72.86	64.17	61.43	51.36	43.18	44.92
D_Hybrid _FBP, %	98.92	98.32	97.77	97.03	95.26	94.73
D_Hybrid _IFBP, %	98.91	98.29	97.64	96.67	94.79	93.91

4. Conclusion

Design principles on modelling the solution for the forward and inverse problems were discussed and structured based on a typical fan-beam transmission mode UT system. Mathematical procedures for dynamic sensitivity check instead of mass load static sensitivity maps were interpreted and samples of transmission paths were discussed. In this paper, the event-driven applications were elaborated with supporting programming flow charts. In the results analysis, images reconstructed in forward and inverse modelling were tabulated and assessed with MSSIM image quality quantitative technique. These first attempts of event-driven modelling applications in UT system are satisfactory with the image reconstruction algorithms of D_Hybrid_FBP and D_Hybrid_IFBP, with high MSSIM results (>90%) of the inverse modelling application. Future work will focus on adding analytical solutions with real hardware performance analysis using these high-quality image algorithms.

References

[1] Raymond, G. and Nancy, K. 1996. A History of the Radiological Sciences. Radiology Centennial. 3(1): 369-401.

[2] Mohd Hafiz bin Fazalul Rahiman. 2005. Non-Invasive Imaging of Liquid/Gas Flow Ultrasonic Transmission-Mode Tomography. M.Sc. Thesis. Universiti Teknologi Malaysia.

[3] Javad, A. 2014. Image Reconstruction Technique via UltrasonicTomography System for Metal Pipe. PhD Thesis. Universiti Teknologi Malaysia.

[4] Chan, K. S. 2002. Real Time Image Reconstruction for Fan Beam Optical Tomography System. M.Sc. Thesis. Universiti Teknologi Malaysia.

[5] Leong, L. C. 2005. Implementation of Multiple Fan Beam Projection Technique in Optical Fibre Process Process Tomography. M.Sc. Thesis. Universiti Teknologi Malaysia.

[6] Mohd Hafiz Fazalul Rahiman. 2013. Ultrasonic Tomography System for Liquid/Gas Bubble Column. Ph.D Thesis. Universiti Teknologi Malaysia.

[7] Jin, J. H. 2008. Industrial Process Gamma Tomography. International Atomic Energy Agency IAEA. 1(1): 1580-1589.

[8] Goh, C. L., Ruzairi, A. R., Hafiz, F. R. 2016. Process tomography of gas-liquid flow in a vessel: a review. Sensor Review, Vol. 36 Iss 3 pp. 287 – 302.

[9] Goh, C. L. 2005. Real-time solids mass flow rate measurement via Ethernet based optical tomography system. M.Sc. Thesis. Universiti Teknologi Malaysia.

[10] Rahiman, M.H.F., Rahim, R.A., Rahim, H.A., Green, R.G., Zakaria, Z., Mohamad, E.J. and Muji, S.Z.M., 2016. An evaluation of single plane ultrasonic tomography sensor to reconstruct three-dimensional profiles in chemical bubble column. Sensors and Actuators A: Physical, 246, pp.18-27.

[11] Yang, W. Q and Peng, L. 2013. Image reconstruction algorithms for electrical capacitance tomography, Measurement Science and Technology. 14(1):120-130.

[12] Hafiz, F. R., Ruzairi, A. R, Herlina, A. R., Siti, Z. M. M. and Elmy, J. M. 2012. Ultrasonic Tomography Image Reconstruction Algorithms. International Journal of Innovative Computing, Information and Control ICIC International. 8(1B): 85-96.

[13] Benjamin Kimia. 2011. Geometry in CT Reconstruction. Technical White Note. Brown University.

[14] Gamio, J. C., Ortiz, C. As. and Martin, R. 2005. Electrical Capacitance Tomography Two-Phase Oil-Gas Pipe Flow Imaging By The Linear Back-Projection Algorithm. Geofisica International. 44(3): 265-273.

[15] Ibrahim, S. 2000. Measurement of Gas Bubbles in a Vertical Water Column Using Optical Tomography. Ph.D. Thesis. Sheffield Hallam University.

[16] Goh, C. L. 2006. Real-Time Solids Mass Flow Rate Measurement via Ethernet based Optical Tomography System. M.Sc Thesis. Universiti Teknologi Malaysia.

[17] Zhou, W., Alan, C. B., Hamid, R. S. and Eero, P. S. 2004. Image Quality Assessment: From Error Visibility to Structural Similarity. IEEE Transactions on Image Processing. 13(4): 1-9.

[18] Zhou, W. and Alan C. B. 2009. Mean Squared Error: Love It or Leave It? A New Look At Signal Fedelity Measures. IEEE Signal Processing Magazine. 1(1): 98 -117.

[19] David, M. R. and Sheila S. H. 2008. Analyzing the Role of Visual Structure in the Recognition of Natural Image Content with Multi-Scale SSIM. SPIE Human Vision and Electronic Imaging XIII. 3(1): 1-21.

[20] Wang, S., Rehman, A., Wang, Z., Ma, S. and Gao, G. 2013. SSIM-inspired Divisive Normalization for Perceptual Video Coding, IEEE Transactions on Image Processing. 22(4): 1418-1429.